Front. Mater. Sci. 2017, 11(3): 250–261
DOI 10.1007/s11706-017-0389-5

RESEARCH ARTICLE

Preparation and characterization of phosphate-modified mesoporous TiO_2 incorporated in a silica matrix and their photocatalytic properties in the photodegradation of Congo red

Alberto ESTRELLA GONZÁLEZ (✉), Maximiliano ASOMOZA, Ulises ARELLANO, Sandra CIPAGAUTA DíAZ, and Silvia SOLÍS

Department of Chemistry, Metropolitan Autonomous University-Iztapalapa, P.O. Box 55-532, C.P. 09340, México City, México

ABSTRACT: This study describes the development of mesostructured TiO_2 photocatalysts modified with PO_4^{3-} to improve its specific surface area and reduce the recombination rate of the electron–hole pairs. The mesoporous photocatalyst was successfully incorporated into a high specific surface area silica matrix by the hydrolysis reaction of tetraethyl orthosilicate (TEOS). Pluronic 123 and phosphoric acid were used as the directing agent for the structure of the mesoporous TiO_2 and as a source of phosphorus, respectively. TiO_2, P/TiO_2, TiO_2–SiO_2 and P/TiO_2–SiO_2 materials were characterized by BET, XRD, TEM-EDS, FTIR and UV-vis DRS measurements. The photoactivity of TiO_2–SiO_2 nanocomposites containing 15 wt.% photocatalyst/silica was evaluated in the degradation reaction of anionic dyes with UV radiation. The proposed nanomaterials showed high potential for applications in the remediation of wastewater, being able to reuse in several cycles of reaction, maintaining its photoactivity and stability. The separation and recovery time of the material is reduced between cycles since no centrifugation or filtration processes are required after the photooxidation reaction.

KEYWORDS: photocatalysis; phosphated TiO_2; TiO_2–SiO_2; Congo red dye

Contents

Received April 28, 2017; accepted June 10, 2017

E-mail: xanum.aeg@gmail.com

1 Introduction

Titanium dioxide (TiO_2) is the most studied semiconductor in photocatalytic reactions and as support of catalysts [1–4]. Its safety, ease of use, resistance to photo-induced corrosion and its low cost are some of the important properties of this material. Because the commercial TiO_2 has a low surface area and a small particle size (52 m^2/g and 12 nm), the recovery of the reaction mixture is difficult, so, for the different applications expected for TiO_2, an increase of the surface area is desirable, although a complete ordered structure is not determinant, due the selectivity is not related with the shape in most of its applications [5–6]. In recent years, the synthesis of mesoporous TiO_2 under different conditions has been extensively studied [7–11]. Mesoporous TiO_2 is a semiconductor that exhibits high photoactivity, related to its large specific surface area, and its ability to activate photocatalytic reactions [12–14]. The thermal treatments at high temperatures necessary to achieve the most active phase of TiO_2 (anatase) generally induce at the recrystallization of the mesoporous structure, as well as the decrease of surface area due to the sintering of the material and growth of the crystal [15].

Among the most used methods to avoid the sintering of the mesoporous structure of TiO_2, doping with phosphorus has attracted attention in recent years [15–20]. Kőrösi et al. [17] prepared a series of samples of phosphate-modified TiO_2 by the sol–gel method. They found that surface phosphate delays the formation of the anatase phase, the growth of the crystallites, and the transformation of the anatase-rutile phase. Lin et al. [18] showed that phosphorous doping can effectively inhibit grain growth and increase the specific area of TiO_2 nanoparticles.

The immobilization of TiO_2 on various substrates is an important research topic for photocatalytic treatment applications of wastewater [21]. The main objective is to avoid the separation difficulties associated with the powder form of the TiO_2 catalyst, other additional advantages of the immobilized systems are: higher specific surface area, higher adsorption properties [22–23], increase of surface hydroxyl groups and reduction of charge recombination (electron–hole) [24].

One of the most studied supports for the immobilization of TiO_2 is silicon dioxide (SiO_2), which is characterized by a large specific surface area, high thermal stability and good sedimentation capacity. Chen et al. [25] reported that the large specific area of SiO_2 potentially improves activity by increase surface available for the reagent, and thus, improving adsorption [26]. In addition, the transparency of SiO_2 allows the photons to penetrate into the mass of the photocatalyst.

In the present work, 15 wt.% of photoactive mesoporous TiO_2, with phosphate and without phosphate were dispersed in a SiO_2 matrix formed by the hydrolysis and condensation reactions of tetraethyl orthosilicate (TEOS) to prepare P/TiO_2–SiO_2 nanocomposites and TiO_2–SiO_2. Silica was selected as matrix to incorporate the photocatalyst, since it presents good light transmission. The structural, optical and chemical properties of the materials related with the photooxidation of anionic dyes in aqueous solution under ultraviolet (UV) irradiation and the reuse of materials in the photodegradation process were investigated.

2 Materials and methods

2.1 Materials

All chemicals were analytical grade and used without further purification in the experiments. Titanium(IV) isopropoxide (Merck) and tetraethyl orthosilicate (Aldrich) were used as the sources for Ti and Si respectively. Triblock copolymer (Pluronic P123, Mw = 5800, $EO_{20}PO_{70}EO_{20}$; Aldrich) and phosphoric acid (J.T. Baker, 85%) were used as the structure directing template and phosphate source respectively. Distilled water and ethanol (J.T. Baker) were used for the preparation of catalyst. Congo red (CR) dye (Aldrich) was used as the test molecule for activity study.

2.2 Synthesis of photocatalysts

2.2.1 Preparation of mesoporous P/TiO_2

Mesoporous P/TiO_2 materials were synthesized by the sol–gel method, using soft template mechanism with Pluronic 123 as the structure directing agent. Pluronic 123 (2g) was dissolved in absolute ethanol (30 mL), then, titanium(IV) isopropoxide (30 mL) were added to it and the mixture was stirred for 2 h. Phosphoric acid (0.3 mL) was added to the

solution to prepare TiO_2 samples with P/TiO_2 ratio of 0.2 (wt.%). The resulting suspension was stirred for 2 h, followed by the addition of deionized water (8 mL) and the stirring continued for another 24 h. The synthesis of the phosphate-free material was performed as described without the addition of phosphoric acid. The prepared samples were calcined at 400°C for 6 h at a heating rate of 1°C/min. The materials were labeled as P/TiO_2 and TiO_2.

2.2.2 Incorporation of P/TiO_2 and TiO_2 photocatalysts into silica matrix

The previously obtained photocatalysts P/TiO_2 and TiO_2 were incorporated into a silica matrix to the weight ratio $w(TiO_2)/w(SiO_2)$ of 15/85, respectively. The procedure is detailed below:

In separate containers for each photoactive material (P/TiO_2 and TiO_2), TEOS and ethanol were mixed in 1:4 molar ratio. The resulting mixture was kept under stirring for 2 h, then, the corresponding mass of each material was added, keeping constant agitation for 1 h, the amount of deionized water required to achieve a final TEOS, ethanol and water ratio of 1:4:2.5 was added, the pH of the solution was adjusted to 5 with HCl, and finally, the temperature was raised to 60°C while maintaining the system at reflux for 12 h. The prepared materials are recovered by filtration, washed with deionized water, dried at 70°C for 24 h, and finally, calcined at 400°C. The synthesized materials were labeled P/TiO_2–SiO_2 and TiO_2–SiO_2. In the nomenclature used P refers to the phosphate material, TiO_2 to the mesoporous material and SiO_2 to the silica matrix.

2.3 Characterization of photocatalysts

The X-ray diffraction (XRD) patterns were recorded on a Siemens D500 X-ray diffractometer using Cu Kα radiation as the X-ray source, in the 2θ range from 10° to 70°. The low-angle XRD patterns of the materials were recorded on a Bruker D8 advanced powder X-ray diffractometer using Cu Kα (λ = 1.5418 Å) as the radiation source in the 2θ range of 0.5°–6°. The UV-visible diffuse reflectance spectroscopy (UV-vis DRS) patterns of samples were obtained using a Varian CARY 100 UV-vis spectrophotometer over a range of 200–600 nm equipped with an integrating sphere and with $BaSO_4$ as the reference. The N_2 adsorption–desorption isotherms were measured at 77 K on a Micromeritics ASAP 2000 analyzer. Prior to each adsorption measurement, the samples were degassed for 2 h at 200°C. The specific surface area was calculated by Brunauer–Emmett–Teller (BET) method, and the pore size distribution was calculated using the Barrett–Joyner–Halenda (BJH) method. The Fourier transform infrared spectroscopy (FTIR) results of the samples were recorded in the range of 4000–400 cm^{-1} on a Perkin Elmer SPECTRUM GX FTIR spectrometer. The morphology of the materials was examined by scanning electron microscopy (SEM) using a SEM-JEOL, JSM-5600 model. The accelerating voltage of the SEM was 20 keV. Transmission electron microscopy (TEM) images were recorded using a JEOL TEM-3010 electron microscope operated at an accelerating voltage of 300 keV.

2.4 Photocatalytic activity

The photodegradation of CR dye was performed in aqueous medium in a photocatalytic reactor. In a typical procedure 200 mg of the photocatalyst was added to 100 mL of CR dye solution (50 mg/L) and the resultant mixture was stirred for 60 min in the dark to ensure adsorption–desorption equilibrium in the probe molecule. The reactor temperature was kept constant at 30°C in all determinations.

The solution was then irradiated with a UV lamp (Pen Ray 2.4 mW, λ = 254 nm) protected with an immersed quartz tube in the solution, the solution was kept under constant stirring. At periodic intervals of 30 min, about 5 mL aliquot were taken to monitored dye degradation from the characteristic absorption band at 498 nm using a Varian Cary 100 UV-vis spectrophotometer in the range of 190–650 nm. The quantification of the total organic carbon was used to determine the extent of mineralization of CR dye using a Shimadzu TOC-V CSN analyzer.

3 Results and discussion

3.1 Characterization results

3.1.1 XRD

XRD diffractograms of TiO_2, P/TiO_2, TiO_2–SiO_2 and P/TiO_2–SiO_2 are show in Fig. 1(a). The TiO_2 and P/TiO_2 samples present the characteristic peaks of the anatase phase (JCPDS, No. 21-1272) at 2θ angles of 25.4° (101), 37.8° (004), 48.1° (200), 54.5° (105) and 62.4° (204), and no characteristic peak of the rutile phase at 2θ angle of 27.4° (110) was observed. The material synthesized only with structure director P123, has an intense main peak of the anatase phase, which is related to the crystallinity of the

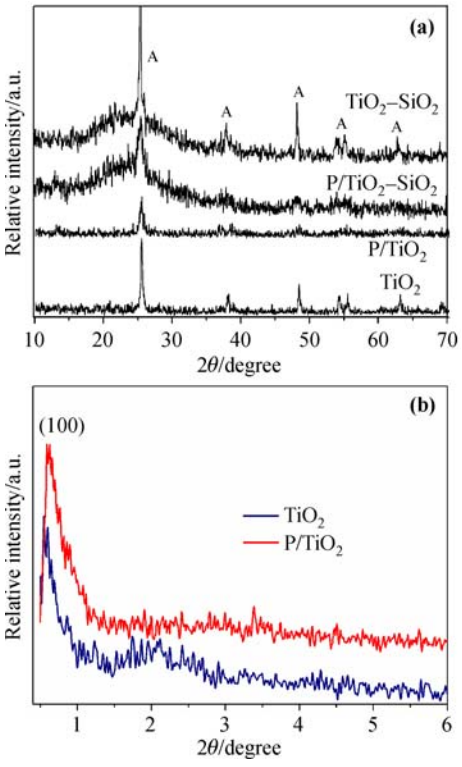

Fig. 1 **(a)** XRD patterns of TiO_2, P/TiO_2, P/TiO_2–SiO_2 and TiO_2–SiO_2 samples. **(b)** Low-angle XRD patterns of TiO_2 and P/TiO_2 samples.

material. These results agree with reported work showing that the addition of P123 structure director has a direct impact on the formation of the anatase phase and the inhibition of rutile phase formation [27]. The diffractogram of the TiO_2 material with addition of phosphoric acid, P/TiO_2 shows a decrease in the intensity of the main peak of the anatase phase at 2θ angle of 25.4° and the half-width of the diffraction peak is broadened, indicating a decrease in the crystallinity of the material and the formation of smaller TiO_2 crystals. The average crystal size was calculated using the Scherrer equation [28]. From the amplification of this peak, corresponding to the (101) plane, the calculated values were 11.4 and 9.1 nm for the materials TiO_2 and P/TiO_2, respectively. As can be observed, the crystallite size became smaller in phospahted material. This result suggests that phosphatation inhibits to a greater degree the growth of TiO_2 crystallites.

For the diffractograms of TiO_2–SiO_2 and P/TiO_2–SiO_2 silica materials, the characteristic amorphous SiO_2 signal was observed, and it consist on a broad pattern of the diffractogram in the 2θ range of 10°–35°. After inclusion of the TiO_2 and P/TiO_2 materials, the characteristic peaks of the anatase phase of TiO_2 are clearly observable, this is attributed to the TiO_2 oxides being homogeneously distributed throughout the photocatalyst which can increase contact and the interactions with the molecules of the contaminant along the photocatalytic reaction, also suggests a good coupling of the photocatalysts in the substrate.

The low-angle XRD patterns of TiO_2 synthesized only with P123 and P123 with phosphate are presented in Fig. 1(b). Both samples show a strong diffraction peak in the low-angle region corresponding to the (100) plane, indicative of the microstructure presence. The intensity of the reflection 100 in the TiO_2 material is lower in comparison with the P/TiO_2 material, and this behavior is related to the decrease in the order of the mesopores in TiO_2 material [27]. The decrease in the mesostructure of TiO_2 compared to the P/TiO_2 material is related probably because of the absence of phosphorus in this material.

It has been reported that wormhole-like mesostructures often display a very intense low-angle XRD peak compared to the other diffraction peaks. The wormhole-like channels that are more or less regular in diameter can form three-dimensional (3D) mesoporous structures. Similar systems have been observed for disordered mesoporous TiO_2 [29].

3.1.2 Energy dispersion X-ray spectroscopy (EDX)

EDX analysis of the samples is presented in Fig. 2. The spectrum of sample P/TiO_2 presented in Fig. 2(a) shows the characteristics signals for Ti, O and the distinctive signal for P at 4.5, 0.5 and 2.1 keV, respectively.

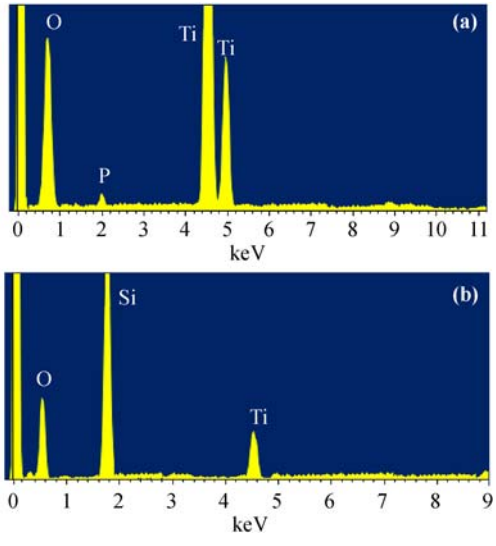

Fig. 2 EDX spectra of **(a)** P/TiO_2 and **(b)** P/TiO_2–SiO_2 samples.

EDX spectrum of the material immobilized on the SiO_2 substrate is presented in Fig. 2(b). Characteristic signals for Si at 1.7 keV, O at 0.5 keV and a lower intensity signal at 4.5 keV, attributed to Ti element can be observed.

The presence of titanium in this material suggests that nanoparticles observed in TEM images (see in Fig. 6) correspond to TiO_2 incorporated in a silica matrix; the phosphorus signal is not observable due the silicon signal.

3.1.3 N_2 adsorption–desorption isotherms (BET)

Figure 3 shows the N_2 adsorption–desorption isotherms of the TiO_2, P/TiO_2, TiO_2–SiO_2, P/TiO_2–SiO_2 materials. The isotherms of the TiO_2 and P/TiO_2 materials are type IV with a hysteresis loop type H_2 evidencing the presence of mesoporous, good connectivity between the pores and the presence of pores with narrow mouths according to the IUPAC classification [30].

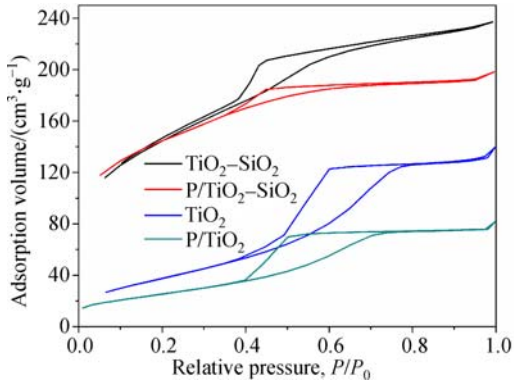

Fig. 3 N_2 adsorption–desorption isotherms of TiO_2, P/TiO_2, TiO_2–SiO_2 and P/TiO_2–SiO_2 materials.

The specific surface area, pore volume and pore diameter are presented in Table 1. The material synthesized with phosphoric acid has a higher surface area than the non-phosphorus TiO_2 material which is attributed to the fact that the incorporation of the phosphate anion was able to stabilize the mesoporous structure of the P/TiO_2 material, avoiding further sintering due to the thermal treatment. The type IV isotherms of the materials incorporated in the silicon matrix TiO_2–SiO_2 and P/TiO_2–SiO_2 indicate that the materials preserve the mesoporous structure of the previously synthesized TiO_2 and P/TiO_2 materials. The specific surface area of the materials was 529 and 497 m^2/g for P/TiO_2–SiO_2 and TiO_2–SiO_2, respectively. These values of specific surface area suggest that the photocatalytic material was successfully dispersed in the translucent silica matrix.

Table 1 The textural parameters of samples

Catalyst	Specific surface area /($m^2 \cdot g^{-1}$)	Pore volume /($cm^3 \cdot g^{-1}$)	Pore diameter /nm
TiO_2	112	0.44	7.7
P/TiO_2	141	0.14	7.1
TiO_2–SiO_2	529	0.34	4.1
P/TiO_2–SiO_2	497	0.29	3.4

3.1.4 UV-vis DRS

UV-vis DRS results of TiO_2, P/TiO_2, TiO_2–SiO_2 and P/TiO_2–SiO_2 samples are included in Fig. 4. The band gap (E_g) values of the materials were obtained with the modified Kubelka–Munk function from the absorption spectra, assuming an indirect transition for TiO_2 as has been reported in numerous articles [31–32]. This method consists in plot of the modified Kubelka–Munk function $[F(R)\cdot h\nu]^{1/2}$ versus $h\nu$, where $F(R) = (1-R)^2/(2R)$ is calculated from the reflectance (defined as R = (1 – Absorbance)) and $h\nu$ is the photon energy in eV [32]. The band gap value is calculated by extrapolating the linear part of the function: the intersection with the x-axis corresponds

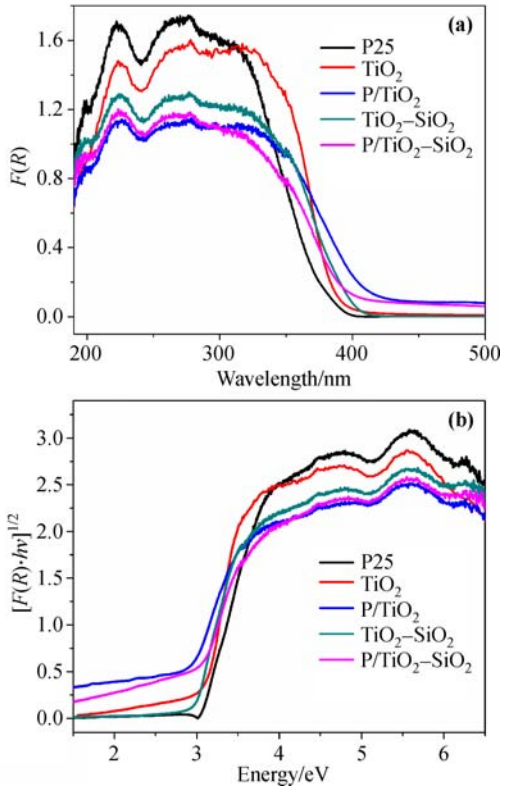

Fig. 4 **(a)** Diffuse reflectance spectra and **(b)** modified Kubelka–Munk spectra of the TiO_2, P/TiO_2, TiO_2–SiO_2 and P/TiO_2–SiO_2 materials.

to the band gap energy. All the materials show a semiconducting behavior that consists of a rise in the absorption edge.

According to Fig. 4(a) a signal corresponding to the isolated Ti at about 225 nm is observed in the spectra of the materials. The absorption peak of 200–260 nm can be attributed to the transfer of electrons from the O_2^- to Ti^{4+} ions of the TiO_2 unit with tetrahedral coordination of the photocatalysts. Yamashita et al. reported that TiO_2 with tetrahedral coordination can be chemically supported on silica matrices and has high photocatalytic activity [33].

The TiO_2 sample shows an edge with absorption around 400 nm, while the P/TiO_2 material showed a shoulder in the range 410–430 nm, reflecting a small displacement in the absorption towards the region of visible radiation, which is attributed to the phosphorus of the material P/TiO_2 [17,27]. The band gap energy values (E_g) calculated for non-included photocatalysts were 3.10 and 2.84 eV for TiO_2 and P/TiO_2, respectively (Fig. 4(b)), which are lower than 3.20 eV evaluated by the reference material Degussa P25. The values calculated for the materials synthesized with 15 wt.% TiO_2 were 3.16 and 3.04 eV for TiO_2–SiO_2 and P/TiO_2–SiO_2, respectively. This observed shift towards lower energy in the photocatalysts incorporated in silica can be indicative of the good incorporation of the material in the support.

3.1.5 FTIR measurements

Figure 5 depicts FTIR spectra of TiO_2, P/TiO_2, TiO_2–SiO_2 and P/TiO_2–SiO_2 materials. The materials TiO_2 and P/TiO_2 show a peak in the region of low energy 500–700 cm^{-1}, which is assigned to Ti – O vibrations and Ti – O – Ti bonds, typical of TiO_2. The presence of Ti ions in a tetrahedral coordination described in the UV-vis DRS

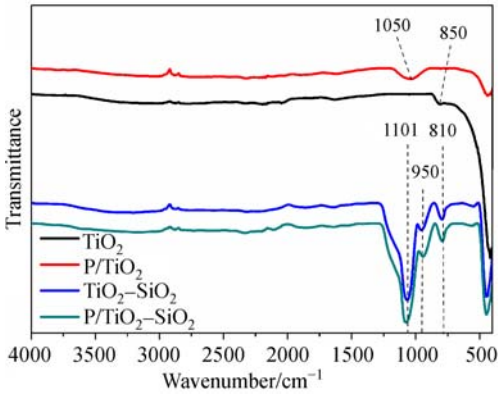

Fig. 5 FTIR results of TiO_2, P/TiO_2, TiO_2–SiO_2 and P/TiO_2–SiO_2 materials.

results are very efficient in the adsorption of water [27]. The band located at 850 cm^{-1} in the TiO_2 material is assigned to the Ti – O – Ti stretch vibration in octahedral coordination. The signal located at 1180–910 cm^{-1} observed in the P/TiO_2 material is related with the characteristics stretching vibrations of PO_4^{3-} groups. The band at 1050 cm^{-1} is related to bound phosphates in bidentate form, the formation of Ti – O – P species is characteristic of a signal at 1125 cm^{-1}.

For the materials TiO_2–SiO_2 and P/TiO_2–SiO_2, the band at 1101 cm^{-1} and the shoulder at 1193 cm^{-1} are associated with asymmetric stretching vibrations of siloxane groups (Si – O – Si). The bands at 470 and 810 cm^{-1} are assigned to symmetrical siloxane groups (Si – O – Si). The 950 cm^{-1} band is associated with Si – OH groups and the presence of silanol groups [34].

The results of FTIR reveal that by addition of phosphoric acid to the TiO_2 mixture, the phosphate ions can react with the OH groups on the surface of TiO_2, resulting in the formation of bonds with the surface. The presence of the groups P – O – Ti, P = O and P – OH indicate that they may be present in the surface as mono-, bi- and tridentate phosphate units.

Additionally, several authors have reported the formation of strong bonds between the bidentate form of phosphates and the TiO_2 surface [17,35]. Connor et al. [35] reported that phosphate species bind to TiO_2 predominantly in bidentate form in neutral and acidic aqueous solution. In our case, the reaction mixture had a pH of about 6.1, therefore the interaction in a form of bidentate bond through P = O is more favorable in P/TiO_2 photocatalyst.

3.1.6 TEM

TEM images of the materials are presented in Fig. 6. Figures 6(a) and 6(b) show evidence of non-agglomerated crystalline domains of size in the range of 10–20 nm. These crystallites are surrounded by amorphous silica matrix visualized by low contrast grey slabs and spots. Figure 6(c) shows crystalline zones, which correspond to the main series of crystalline interplanar distances measured from HRTEM images (Fig. 6(d)) resulting in: d_1 = 0.354 nm, which conforms to the anatase TiO_2 polymorph (101) [36].

The crystallite size of the materials estimated from the TEM images agrees with the sizes calculated using the Scherrer equation in the XRD patterns. Figure 7 shows the distribution of O, Ti, and Si; the elements Ti and Si incorporated are uniformly distributed in the matrix, which

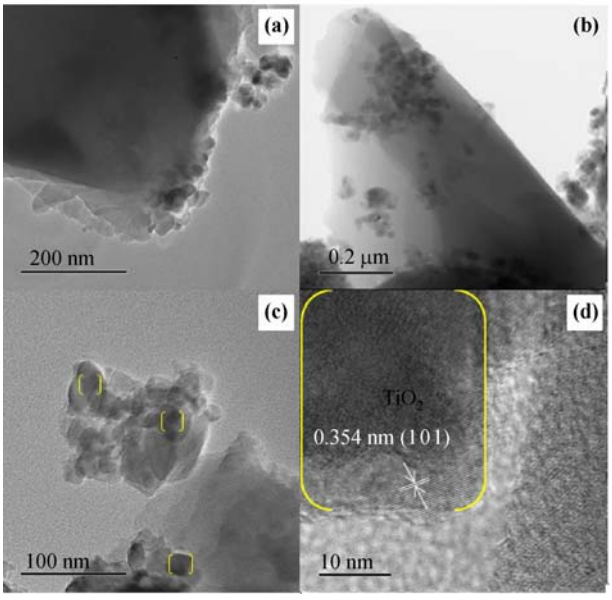

Fig. 6 **(a)(b)(c)** TEM images and **(d)** HRTEM image of the sample TiO_2/SiO_2.

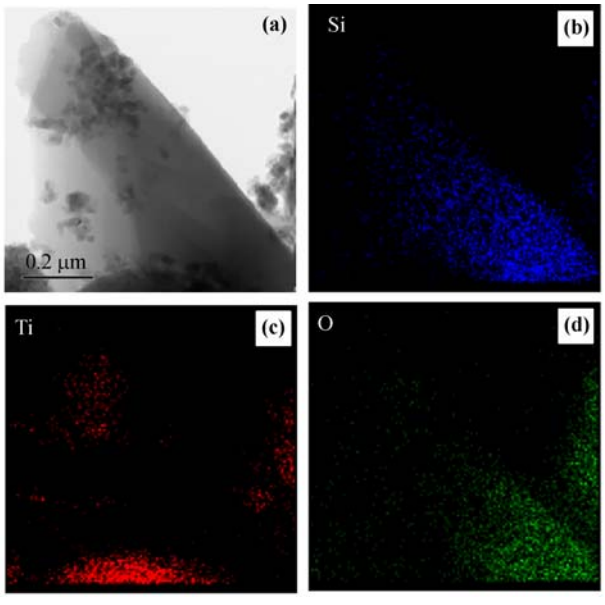

Fig. 7 **(a)** TEM image and **(b)(c)(d)** elemental mapping of the TiO_2–SiO_2 material.

is indicative that the synthesis method avoided the agglomeration of TiO_2 and allowed the incorporation of the photocatalyst into the silica matrix.

3.2 Photocatalytic activity

The photocatalytic activity of the samples was analyzed by the degradation of CR dye in the presence of UV light. Before assessing and comparing the activities, some control experiments were performed. By means of experiments it is concluded that less than 5% of CR dye decomposes after 4 h in the absence of the photocatalyst or the light irradiation (photolysis) and can therefore be discarded in comparison with the degraded dye through the photocatalysis. The photocatalytic activity of the reference material Degussa P25 was measured under conditions identical to those detailed in the experimental section in order to compare the activity of our materials.

Figure 8 presents the comparative degradation of CR using P/TiO_2, TiO_2, P/TiO_2–SiO_2, TiO_2–SiO_2 and Degussa P25 materials. When exposed to the radiation, P/TiO_2–SiO_2 and TiO_2–SiO_2 gave complete degradation of CR within 4 h. From the graph, it was noted that P/TiO_2, TiO_2, P/TiO_2–SiO_2, TiO_2–SiO_2 and Degussa P25 materials were able to degrade 98%, 95%, 88%, 82% and 93% of CR dye, respectively. Moreover, among all the samples, the maximum photocatalytic activity was observed with the P/TiO_2 photocatalyst.

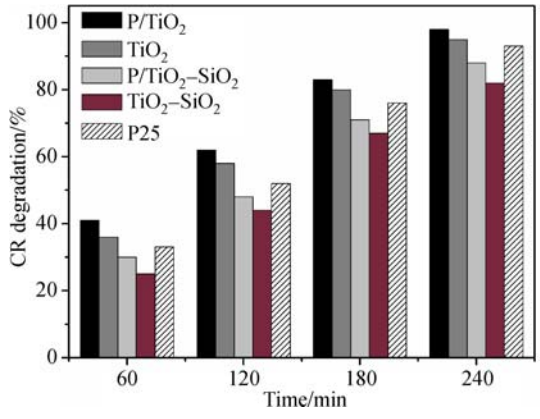

Fig. 8 Percentages of degradation of aqueous CR dye with materials.

The photocatalytic performance of TiO_2–SiO_2 and P/TiO_2–SiO_2 materials showed to be very close to that of bare commercial TiO_2 Degussa P25. It is important to note that the high activity of the photocatalysts incorporated in the silica matrix shown in Fig. 9 is achieved using a weight ratio $w(TiO_2)/w(SiO_2)$ of 15/85 in the final TiO_2–SiO_2 and P/TiO_2–SiO_2 materials. The photocatalytic activity of materials immobilized in SiO_2 are closely related to its large surface area which may offer more sites to absorb the hydroxyl groups generated during the reaction and the ease of diffusion of the reactants in the mesopores of TiO_2–SiO_2 and P/TiO_2–SiO_2 materials. Furthermore, the oxidative reaction of CR dye is believed to be initiated by ·OH radicals [37–38], therefore the surface-adsorbed water and

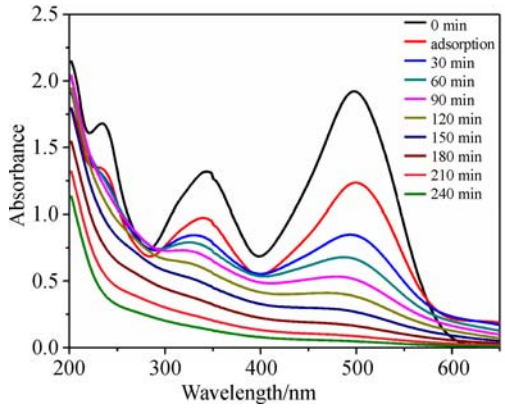

Fig. 9 UV spectra of the aqueous CR dye degradation with the P/TiO_2–SiO_2 photocatalyst.

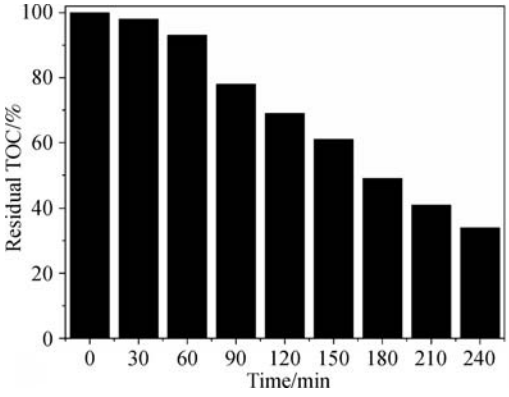

Fig. 10 The residual TOC in the photodegradation of aqueous CR dye with the P/TiO_2–SiO_2 material after 4 h.

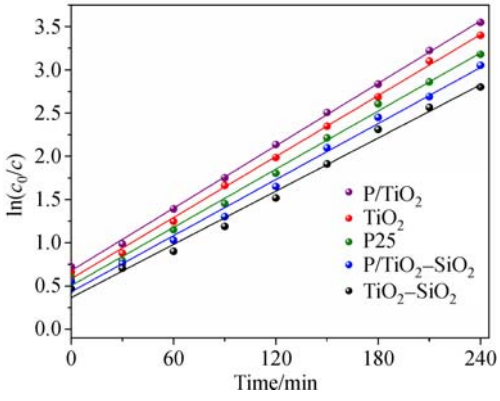

Fig. 11 Plots of the pseudo-first order kinetics of CR photodegradation.

hydroxyl groups can react with photogenerated holes on the catalyst surface and produce hydroxyl radicals, which are powerful oxidants in degrading organics [27].

Figure 9 shows UV spectra of the CR dye at different reaction times with the P/TiO_2–SiO_2 photocatalyst. The adsorption stage of dye on the surface of photocatalyst was recorded in dark conditions, with a value of 25% of the initial concentration of the solution (50 mg/L). Since the pre-adsorption of the dye on the surface of the photocatalysts is an important factor for the photodegradation of contaminants under light irradiation; a higher adsorption will improve the degradation. In addition, the specific surface of SiO_2 matrix will contribute to improve the accessibility of the dye to the surface, and the radiation will penetrate more efficiently to influence a larger number of Ti^{4+} metal cations, generating more electron–hole pairs (e^-–h^+) [25].

Figure 9 show that the intensity of the main absorption band at 484 nm due to the chromophore decreased 98% in 240 min of photoreaction in the presence of the P/TiO_2–SiO_2 photocatalyst, because of the degradation of CR dye.

In the absorption spectrum, no new band is present in the UV-vis region; this observed behavior is attributed to the photodegradation of the chromophore, responsible of the characteristic CR dye color.

Figure 10 shows the evaluation of the total organic carbon (TOC) with the catalyst P/TiO_2–SiO_2. The amount of TOC decreases to a 34% during 240 min of reaction, indicating the mineralization of the CR dye molecule to simple molecules (CO_2 and H_2O) by the action of photocatalyst.

Figure 11 shows that the photocatalytic degradation of CR dye follows the pseudo-first order kinetics represented by Eq. (1):

$$\ln\left(\frac{c_0}{c}\right) = k_{app}t \tag{1}$$

where c_0 is the initial concentration of the dye, c is the concentration at time t, and k_{app} is the apparent rate constant.

A plot of $\ln(c_0/c)$ as a function of the reaction time provides the apparent rate constants for the CR dye degradation. From the slope of the curve fitting line and the intersection point equal to zero, the apparent rates constants was found to be 0.0120, 0.0116, 0.0109, 0.0104 and 0.0098 min^{-1} for P/TiO_2, TiO_2, P25, P/TiO_2–SiO_2 and TiO_2–SiO_2, respectively.

3.3 Mechanism of the CR dye photodegradation

The absorption spectrum of the CR dye solution is characterized by a band in the visible region with a maximum absorption at 496 nm related to the azo bonds of the CR dye molecule and by two other bands in the UV region located at 235 and 338 nm (Fig. 9), attributed to the

benzene and naphthalene ring structures, respectively [39]. Throughout the course of the CR dye photoxidation reaction, the absorbance decreases and no peaks are observed at 496 nm after 240 min of reaction, almost complete degradation of the dye was achieved, which can be attributed to the breaking of the azo bonds by attack of the generated species in the photocatalyst [40]. The decrease in absorbance in the bands located at 235 and 338 nm can be ascribed to the degradation of the aromatic groups in the CR dye molecule, as well as their intermediates generated since no new peaks in the spectrum are observed. The reduction rates of the three characteristic peaks of the test molecule in the presence of the composite material that presented the best photocatalytic performance P/TiO_2–SiO_2 can be compared in terms of their pseudo-first order rate constants [40–41]. In Fig. 12, the highest decrease of the visible band, k_{app} = 0.0141 min^{-1}, is attributed to the breakage of azo bonds during discoloration and photocatalytic degradation. Thus, it can be concluded that azo bonds N≡N are more susceptible to degradation by hydroxyl radicals than the aromatic rings resulting in the rapid disappearance of the chromophore in the CR dye structure.

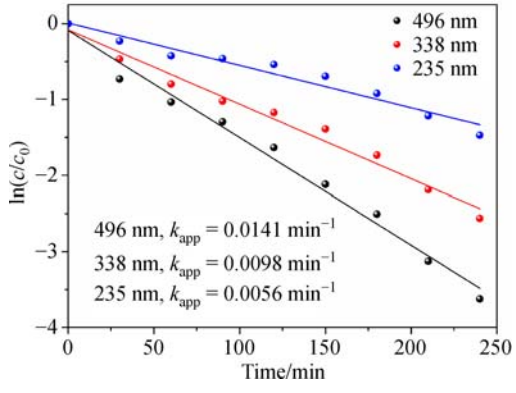

Fig. 12 Photocatalytic behavior of characteristic peaks of CR during the irradiation time with UV light.

The values of k_{app} at 235 and 338 nm are 0.0056 and 0.0098 min^{-1}, respectively, which indicate that the aromatic structures of CR dye were eliminated during the reaction, because of the TiO_2 photocatalysts incorporated into the SiO_2 matrix. This is in agreement with the results obtained in the TOC study, with a significant decrease of the organic groups.

In the case of the P/TiO_2 material, the modification of the TiO_2 structure with phosphate ions seems to be responsible for the improved CR photooxidation. On the one side, the phosphate ions on the surface of the catalyst, can reduce the recombination rate of the photogenerated pairs (e^-–h^+), due to their ability to trap holes, which in turn are capable of converting OH groups, in species highly reactive (·OH), which react with the adsorbed organic compounds, resulting in improved photooxidation. Additionally it improves the structural properties of TiO_2 (stabilization of the anatase phase and improves surface area).

The SiO_2 support can affect both, the conservation of the gap at the interface and the photon losses due to absorption in the volume of the photocatalyst, the Ti centers of the material localized in the surface or at the surface layer which facilitates the reactions of charge transfer with the molecules of the adsorbed contaminant. The synthesis of the nanomaterial composed of P/TiO_2 particles previously synthesized and deposited in the SiO_2 matrix with a relatively low concentration (15 wt.%), allows the coverage of only a small fraction of the internal surface of the support, as a result, the particles are not agglomerated during the synthesis process, but may react with the hydroxyl groups that are located on the surface of the pores along the photocatalytic reaction. These factors can explain for the increased activity observed in TiO_2–SiO_2 and P/TiO_2–SiO_2 materials. A proposal of the before mentioned model is presented in Fig. 13.

3.4 Recycling test for the P/TiO_2–SiO_2 material

The recycling of the catalyst in photocatalytic applications is an importance topic, since it can contribute towards to the reduction of costs of the dye wastewater treatment. The experiments were run in consecutive tests once the catalyst was recovered by filtration and a fresh amount of contaminant solution was placed in the reactor. It is important to mention the absence of subsequent treatments such as washes or heat treatments to carry out the cleaning of active sites on the surface of the catalyst. Figure 14 shows the test of photocatalyst P/TiO_2–SiO_2. A degradation of 48.3 mg/L of the initial concentration of CR dye (50 mg/L) elapsed the first cycle and a degradation of 39.8 mg/L after the fifth cycle is observed. The photodegradation efficiency observed during the entire recycling test indicates that the photocatalyst P/TiO_2–SiO_2 shows stability, without aggregation and retaining its surface reactivity properties.

The recycling of the nanocomposites is derived from the separation of the SiO_2 layers, which prevent the aggregation of the active centers and the breakdown of the composite structure during the catalytic reactions. The recycling experiments results suggest the practical applic-

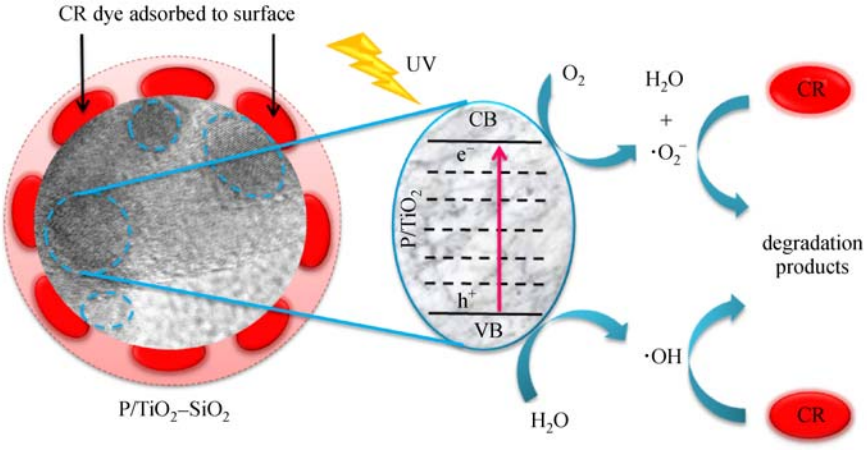

Fig. 13 Schematic illustration of the proposed mechanism for photodegradation of CR dyes by the electron–hole model.

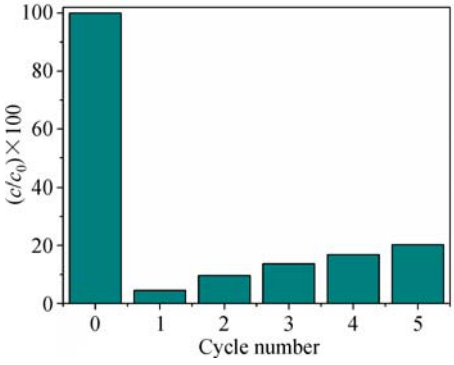

Fig. 14 Recycling and photocatalytic stability studies with the P/TiO_2–SiO_2 material for five cycles under the same experimental conditions.

ability of the TiO_2 materials incorporated in SiO_2 in environmental applications such as water remediation. Finally by stopping the stirring of the solution in the reactor, the photocatalysts P/TiO_2–SiO_2 sediment 90%–95% after 25 min of the reaction is over, while the reference material P25 continues in the mixture of reaction. This feature of the materials proposed in this work, allows the reuse more efficiently than commercial photocatalysts commonly use.

4 Conclusions

The incorporation of the structure director and the phosphoric acid slow the formation of the anatase phase, avoided the collapse of the mesoporous structure and increased the specific surface area of the photocatalysts. Furthermore phosphate modification of the TiO_2 enhances charge separation.

The TiO_2 materials incorporated in the silica matrix showed good adsorption capacity and a high degree of dispersion of the active phase.

The rate of photodegradation of CR dye using materials containing 15 wt.% TiO_2–SiO_2 was similar to that of the Degussa P25 material, which is a relevant factor in large-scale environmental remediation processes. The specific surface area and the adsorption capacity of the P/TiO_2 and TiO_2 materials included in the SiO_2 matrix contributed significantly to the increase in the rate of the CR dye photodegradation. The results of this work show that the materials included in the SiO_2 matrix presented good photoactivity, sedimentation, recovery and recycling capacity in successive cycles of reaction; factors that are of great importance for the use of large-scale photocatalytic systems.

Acknowledgements We thank the National Science and Technology Council of Mexico (CONACYT) for the Scholarship No. 313880. We are very grateful to Victor Hugo Lara and Patricia Castillo for their timely and professional technical assessment in several of the experimental techniques employed in this work.

References

[1] Fujishima A, Honda K. Electrochemical photolysis of water at a semiconductor electrode. Nature, 1972, 238(5358): 37–38

[2] Han F, Kambala V S R, Srinivasan M, et al. Tailored titanium dioxide photocatalysts for the degradation of organic dyes in wastewater treatment: A review. Applied Catalysis A: General, 2009, 359(1–2): 25–40

[3] Reddy K M, Manorama S V, Reddy A R. Bandgap studies on anatase titanium dioxide nanoparticles. Materials Chemistry and Physics, 2003, 78(1): 239–245

[4] Mo S D, Ching W Y. Electronic and optical properties of three phases of titanium dioxide: Rutile, anatase, and brookite. Physical Review B: Condensed Matter and Materials Physics, 1995, 51 (19): 13023–13032

[5] Pekakis P A, Xekoukoulotakis N P, Mantzavinos D. Treatment of textile dyehouse wastewater by TiO_2 photocatalysis. Water Research, 2006, 40(6): 1276–1286

[6] Almquist C B, Biswas P. Role of synthesis method and particle size of nanostructured TiO_2 on its photoactivity. Journal of Catalysis, 2002, 212(2): 145–156

[7] Yoshitake H, Sugihara T, Tatsumi T. Preparation of Wormhole-like mesoporous TiO_2 with an extremely large surface area and stabilization of its surface by chemical vapor deposition. Chemistry of Materials, 2002, 14(3): 1023–1029

[8] Soler-Illia G J D A, Sanchez C. Interactions between poly (ethylene oxide)-based surfactants and transition metal alkoxides: their role in the templated construction of mesostructured hybrid organic–inorganic composites. New Journal of Chemistry, 2000, 24(7): 493–499

[9] Soler-Illia G J D A, Scolan E, Louis A, et al. Design of mesostructured titanium oxo based hybrid organic–inorganic networks. New Journal of Chemistry, 2001, 25(1): 156–165

[10] Calleja G, Serrano D P, Sanz R, et al. Study on the synthesis of high-surface-area mesoporous TiO_2 in the presence of nonionic surfactants. Industrial & Engineering Chemistry Research, 2004, 43(10): 2485–2492

[11] Calleja G, Serrano D P, Sanz R, et al. Mesostructured SiO_2-doped TiO_2 with enhanced thermal stability prepared by a soft-templating sol–gel route. Microporous and Mesoporous Materials, 2008, 111 (1–3): 429–440

[12] Wang W, Lu C, Ni Y, et al. Enhanced performance of {001} facets dominated mesoporous TiO_2 photocatalyst composed of high-reactive nanocrystals and mesoporous spheres. Applied Surface Science, 2013, 265: 438–442

[13] Zhao Z, Sun Z, Zhao H, et al. Phase control of hierarchically structured mesoporous anatase TiO_2 microspheres covered with {001} facets. Journal of Materials Chemistry, 2012, 22(41): 21965–21971

[14] Ismail A A, Bahnemann D W, Robben L, et al. Palladium doped porous titania photocatalysts: impact of mesoporous order and crystallinity. Chemistry of Materials, 2010, 22(1): 108–116

[15] Wang Z C, Shui H F. Effect of PO_4^{3-} and PO_4^{3-}–SO_4^{2-} modification of TiO_2 on its photocatalytic properties. Journal of Molecular Catalysis A: Chemical, 2007, 263(1–2): 20–25

[16] Shi Q, Yang D, Jiang Z, et al. Visible-light photocatalytic regeneration of NADH using P-doped TiO_2 nanoparticles. Journal of Molecular Catalysis B: Enzymatic, 2006, 43(1–4): 44–48

[17] Kőrösi L, Dékány I. Preparation and investigation of structural and photocatalytic properties of phosphate modified titanium dioxide. Colloids and Surfaces A: Physicochemical and Engineering Aspects, 2006, 280(1–3): 146–154

[18] Lin L, Lin W, Xie J L, et al. Photocatalytic properties of phosphor-doped titania nanoparticles. Applied Catalysis B: Environmental, 2007, 75(1–2): 52–58

[19] Yu H F, Zhang Z W, Hu F C. Phase stabilities and photocatalytic activities of P/Zn–TiO_2 nanoparticles able to operate under UV-vis light irradiation. Journal of Alloys and Compounds, 2008, 465(1–2): 484–490

[20] Li F, Jiang Y, Xia M, et al. Effect of the P/Ti ratio on the visible-light photocatalytic activity of P-doped TiO_2. The Journal of Physical Chemistry C, 2009, 113(42): 18134–18141

[21] Shan A Y, Ghazi T I M, Rashid S A. Immobilisation of titanium dioxide onto supporting materials in heterogeneous photocatalysis: A review. Applied Catalysis A: General, 2010, 389(1–2): 1–8

[22] Zhu B, Zou L. Trapping and decomposing of color compounds from recycled water by TiO_2 coated activated carbon. Journal of Environmental Management, 2009, 90(11): 3217–3225

[23] Jin L, Dai B. TiO_2 activation using acid-treated vermiculite as a support: Characteristics and photoreactivity. Applied Surface Science, 2012, 258(8): 3386–3392

[24] Stathatos E, Papoulis D, Aggelopoulos C A, et al. TiO_2/palygorskite composite nanocrystalline films prepared by surfactant templating route: synergistic effect to the photocatalytic degradation of an azo-dye in water. Journal of Hazardous Materials, 2012, 211–212: 68–76

[25] Chen Y, Wang K, Lou L. Photodegradation of dye pollutants on silica gel supported TiO_2 particles under visible light irradiation. Journal of Photochemistry and Photobiology A: Chemistry, 2004, 163(1–2): 281–287

[26] Li Y, Kim S J. Synthesis and characterization of nano titania particles embedded in mesoporous silica with both high photocatalytic activity and adsorption capability. The Journal of Physical Chemistry B, 2005, 109(25): 12309–12315

[27] Yu J C, Zhang L, Zheng Z, et al. Synthesis and characterization of phosphated mesoporous titanium dioxide with high photocatalytic activity. Chemistry of Materials, 2003, 15(11): 2280–2286

[28] Monshi A, Foroughi M R, Monshi M R. Modified Scherrer equation to estimate more accurately nano-crystallite size using XRD. World Journal of Nano Science and Engineering, 2012, 2 (3): 154–160

[29] Yu J C, Zhang L Z, Yu J G. Rapid synthesis of mesoporous TiO_2 with high photocatalytic activity by ultrasound-induced agglomeration. New Journal of Chemistry, 2002, 26(4): 416–420

[30] Thommes M, Kaneko K, Neimark A V, et al. Physisorption of gases, with special reference to the evaluation of surface area and pore size distribution (IUPAC Technical Report). Pure and

Applied Chemistry, 2015, 87(9–10): 1051–1069

[31] Nadtochenko V, Denisov N, Gorenberg A, et al. Correlations for photocatalytic activity and spectral features of the absorption band edge of TiO_2 modified by thiourea. Applied Catalysis B: Environmental, 2009, 91(1–2): 460–469

[32] Tauc J, Grigorovici R, Vancu A. Optical properties and electronic structure of amorphous germanium. physica status solidi, 1966, 15 (2): 627–637

[33] Yamashita H, Ichihashi Y, Harada M, et al. Photocatalytic degradation of 1-Octanol on anchored titanium oxide and on TiO_2 powder catalysts. Journal of Catalysis, 1996, 158(1): 97–101

[34] Rahman I A, Vejayakumaran P, Sipaut C S, et al. Size-dependent physicochemical and optical properties of silica nanoparticles. Materials Chemistry and Physics, 2009, 114(1): 328–332

[35] Connor P A, McQuillan A J. Phosphate adsorption onto TiO_2 from aqueous solutions: an *in situ* internal reflection infrared spectroscopic study. Langmuir, 1999, 15(8): 2916–2921

[36] Pucher P, Benmami M, Azouani R, et al. Nano-TiO_2 sols immobilized on porous silica as new efficient photocatalyst. Applied Catalysis A: General, 2007, 332(2): 297–303

[37] Lachheb H, Puzenat E, Houas A, et al. Photocatalytic degradation of various types of dyes (Alizarin S, Crocein Orange G, Methyl Red, Congo Red, Methylene Blue) in water by UV-irradiated titania. Applied Catalysis B: Environmental, 2002, 39(1): 75–90

[38] Zhu H, Jiang R, Xiao L, et al. Photocatalytic decolorization and degradation of Congo Red on innovative crosslinked chitosan/nano-CdS composite catalyst under visible light irradiation. Journal of Hazardous Materials, 2009, 169(1–3): 933–940

[39] Wang J, Li R, Zhang Z, et al. Efficient photocatalytic degradation of organic dyes over titanium dioxide coating upconversion luminescence agent under visible and sunlight irradiation. Applied Catalysis A: General, 2008, 334(1–2): 227–233

[40] Ince N H, Tezcanlí G. Reactive dyestuff degradation by combined sonolysis and ozonation. Dyes and Pigments, 2001, 49(3): 145–153

[41] Iida Y, Kozuka T, Tuziuti T, et al. Sonochemically enhanced adsorption and degradation of methyl orange with activated aluminas. Ultrasonics, 2004, 42(1–9): 635–639